Threshold current of field-free perpendicular magnetization switching using anomalous spin-orbit torque

Tianyi Zhang,[1] Caihua Wan,[1,2,*] and Xiufeng Han[1,2,3,†]

[1]*Beijing National Laboratory for Condensed Matter Physics, Institute of Physics, Chinese Academy of Sciences, Beijing 100190, China*

[2]*Center of Materials Science and Optoelectronics Engineering, University of Chinese Academy of Sciences, Beijing 100049, China*

[3]*Songshan Lake Materials Laboratory, Dongguan, Guangdong 523808, China*

(Received 6 April 2023; revised 9 June 2023; accepted 12 July 2023; published 27 July 2023)

Spin-orbit torque (SOT) is a promising technique for next-generation magnetic random-access memory. Recent experiments have shown that materials with low-symmetry crystalline or magnetic structures can generate anomalous SOT with an out-of-plane component, which is crucial for switching the perpendicular magnetization of adjacent ferromagnetic (FM) layers in a field-free condition. In this study, we derive the threshold current for field-free perpendicular magnetization switching using anomalous SOT and numerically calculate the magnetic moment trajectory in an FM free layer for currents smaller and greater than the threshold. We also investigate the dependence of switching time and energy consumption on applied current, finding that the minimum energy consumption decreases with an increasing out-of-plane torque proportion. Additionally, we explore the relationships between the threshold current and anisotropy strength, out-of-plane torque proportion, FM free-layer thickness, and Gilbert damping constant. The results show a negative correlation between the threshold current and out-of-plane torque proportion, and positive correlations with the other three parameters. Finally, we demonstrate that even when the applied current is smaller than the threshold current, it can still add an effective exchange bias field H_{bias} on the FM free layer. The H_{bias} is proportional to the applied current J_{SOT}, facilitating the determination of anomalous SOT efficiency. Our findings provide insights into the design of spintronic devices that favor field-free switching of perpendicular magnetization using anomalous SOT and offer a means of adjusting the exchange bias field to control FM layer magnetization depinning.

DOI: 10.1103/PhysRevB.108.014432

I. INTRODUCTION

The spin-orbit torque (SOT) is a promising technique for developing the next-generation magnetic random-access memory (MRAM) [1–6]. Perpendicularly magnetized ferromagnetic (FM) layers have superior performance in thermostability, high density, and retention compared to in-plane magnetized FM layers when used in MRAM [7]. However, ordinary SOT cannot easily switch the perpendicular FM films in the field-free condition. Therefore, deterministically switching the perpendicular magnetization of the FM free layer in magnetic tunnel junctions (MTJs) by SOTs has long been a frontier of SOT studies. According to the spin Hall effect [4], when electron current $\mathbf{j_c}$ is sourced along the x direction, the spin current $\mathbf{j_s}$ transports along the z direction and its polarization $\sigma \propto \mathbf{j_s} \times \mathbf{j_c}$ will be along the y direction. The adjacent FM free layer is thus affected by the spin current dominating through a dampinglike SOT $\tau_{\mathbf{d}} \propto (\mathbf{m} \times \sigma) \times \mathbf{m}$, which is also along the y direction. This torque is orthogonal to the perpendicular easy axis of the free layer; therefore, using pure SOT alone, we cannot deterministically switch the perpendicular magnetization. Several attempts have been made to circumvent this problem, such as applying an in-plane magnetic field [8,9], using structural asymmetry [10,11], mediating an in-plane exchange bias/coupling field [12–17], mediating the interlayer Dzyaloshinskii-Moriya interaction [18], or exploring materials with low-symmetric crystalline or magnetic structures to generate an anomalous SOT [12,19–24].

Specifically, the groundbreaking studies on low-symmetry materials have shown that the spin polarization, denoted by σ, of an out-of-plane transporting spin current $\mathbf{j_s}$ can have both in-plane and out-of-plane components, despite being generated by an in-plane electron current $\mathbf{j_c}$. These crystallized materials include Mn_3Ir [12], Mn_3Pt [20], Mn_3Sn [21], WTe_2 [22], CuPt [25], $MnPd_3$ [26], and more. This anomalous SOT is highly dependent on the crystal or magnetic symmetry. By utilizing the out-of-plane component of σ, one can achieve a deterministic switch of the perpendicular magnetization of a FM free layer without an external magnetic field.

In order to gain a more thorough understanding of the anomalous SOT and its potential for switching a perpendicular magnetization, it is necessary to optimize and utilize relevant parameters that affect the switching dynamics. An analytical derivation of the threshold current in the coexistence of ordinary and anomalous SOTs would be particularly beneficial for this purpose. Despite previous work on formulating threshold currents for other SOT modes [27–31], there is still

*wancaihua@iphy.ac.cn
†xfhan@iphy.ac.cn

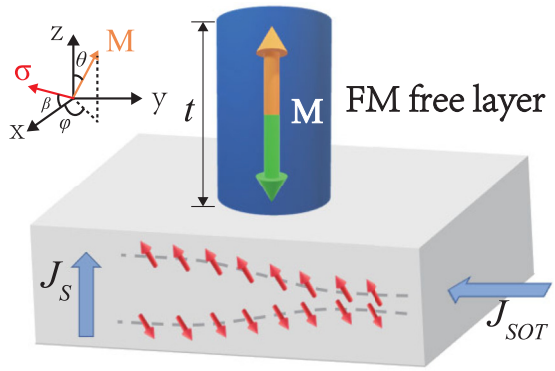

FIG. 1. A schematic diagram of the FM free-layer magnetization switch driven by an anomalous SOT with both in-plane and out-of-plane components. The applied electron current $\mathbf{J}_{\mathrm{SOT}}$ is along the $-y$ direction and generates a spin current $\mathbf{J_S}$ propagating along the z direction. The spin current diffuses into the FM free layer with the perpendicular magnetic anisotropy to drive its magnetization dynamics.

a lack of a specific one for the coexistence case of the anomalous and ordinary SOTs. This research aims to address this gap.

In this paper, we analytically derive the threshold current required to generate an anomalous SOT for switching the perpendicular magnetization of an adjacent FM layer. Additionally, we use macrospin simulations to investigate the precessional trajectory of the FM layer's magnetic moment both below and above the threshold, finding consistent results with our analytical model. We also examine the dependence of switching time and energy consumption on the applied current, as well as the minimum energy consumption dependence on the proportion of the out-of-plane torque. Furthermore, we calculate the threshold current's dependence on anisotropy strength, out-of-plane torque ratio, FM free-layer thickness, and Gilbert damping constant. Finally, we demonstrate that an applied current below the threshold can still produce an effective exchange bias field in the FM layer, and provide the relationship between the effective exchange bias field and the applied current. This work can be instructive to design SOT devices with the anomalous SOT materials.

II. MODEL AND METHOD

The schematic diagram of a FM free-layer magnetization switching driven by the anomalous SOT is shown in Fig. 1. The FM free layer with perpendicular magnetic anisotropy is adjacent to a material with low-symmetric crystalline or magnetic structures. The applied electron current $\mathbf{J}_{\mathrm{SOT}}$ is along the $-y$ direction, spin current $\mathbf{J_S}$ is along the z direction, and the polarization σ of the spin current has components in both x and z directions as shown in the upper left panel of Fig. 1. β is the angle between σ and the x axis. At the interface of the low-symmetric material with the FM free layer, a pure spin current with the σ polarization diffuses into the FM free layer and acts as a dampinglike SOT on the latter. Then the magnetization of the FM layer will precess around an effective magnetic field or switch its magnetization under the concerted interplay of the SOT with other torques from built-in fields.

The spin dynamics of the FM layer can be described by the LLGS (Landau-Lifshitz-Gilbert-Slonczewski) formula [32]

$$\frac{\partial \mathbf{m}}{\partial t} = -\gamma\mu_0(\mathbf{m}\times\mathbf{H_K}) + \alpha\left(\mathbf{m}\times\frac{\partial \mathbf{m}}{\partial t}\right) + \gamma\mu_0 H_{\mathrm{SOT}}^{DL}[(\mathbf{m}\times\sigma)\times\mathbf{m}] \tag{1}$$

where $\mathbf{m} = \frac{\mathbf{M}}{M_s}$ is the unit vector along the direction of magnetization, $\mathbf{M}$ is magnetic moment, M_s is the saturated magnetization value, $\gamma = 1.76\times10^{11}$ $\mathrm{T^{-1}}$ $\mathrm{s^{-1}}$ is the gyromagnetic ratio, $\mu_0 = 4\pi\times10^{-7}$ V s $\mathrm{A^{-1}}$ $\mathrm{m^{-1}}$ is the permeability of vacuum, $\mathbf{H_K} = H_K m_z \mathbf{e_z}$ is the anisotropic field, α is the Gilbert damping constant, $\sigma = (\sigma_x, 0, \sigma_z) = (\cos\beta, 0, \sin\beta)$ is the unit vector along the electron spin polarization direction, β is the angle between the spin polarization direction and the x axis, H_{SOT}^{DL} is the effective field generated by SOT, which can be calculated by the following formula [33–37]:

$$H_{\mathrm{SOT}}^{DL} = \frac{J_{\mathrm{SOT}}\theta_{SH}\hbar}{2et\mu_0 M_s}, \tag{2}$$

where J_{SOT} is the magnitude of the applied electron current density, θ_{SH} is the spin Hall angle that represents conversion efficiency from electron current to spin current, $\hbar = 1.05\times10^{-34}$ J s is the reduced Planck constant, $e = 1.6\times10^{-19}C$ is the elementary charge carried by an electron, and t is the effective thickness of the free layer after subtracting a dead layer if any.

When a small current is applied, the anomalous SOT acting on the FM free layer is not large enough to switch the magnetization of the FM layer. The magnetization will precess under the SOT effect, and stabilize to a final direction due to the Gilbert damping. This direction is so-called the direction of the effective field $\mathbf{H}_{\mathrm{eff}}$. Here we constrain ourself in a field-free system, which is exactly needed in practice. When the applied current is above a threshold $\mathbf{J_c}$, the torque acting on the FM free layer becomes large enough to make the magnetization precession amplitude divergently increase and finally realize magnetization reversal. In the following, we will give the analytical derivation of the threshold current $\mathbf{J_c}$. For those readers who mainly have interest in the dependence of $\mathbf{J_c}$ on various material parameters, they can directly skip to Eq. (15) where the final results are directly given out.

By crossing $\mathbf{m}$ left at both sides of Eq. (1), we can reform the LLGS formula, Eq. (1), as in Eq. (3),

$$\frac{\partial \mathbf{m}}{\partial t} = \frac{-\gamma\mu_0}{1+\alpha^2}\big[(\mathbf{m}\times\mathbf{H_K}) + \alpha\mathbf{m}\times(\mathbf{m}\times\mathbf{H_K}) - H_{\mathrm{SOT}}^{DL}[(\mathbf{m}\times\sigma)\times\mathbf{m}] - \alpha H_{\mathrm{SOT}}^{DL}(\mathbf{m}\times\sigma)\big]. \tag{3}$$

Letting $\frac{\partial \mathbf{m}}{\partial t} = 0$ we can get

$$\mathbf{m}\times\mathbf{H}_{\mathrm{eff}} = 0, \tag{4}$$

where the effective magnetic field $\mathbf{H}_{\text{eff}}$ can be written as

$$\begin{aligned}\mathbf{H}_{\text{eff}} &= \mathbf{H}_K - H_{\text{SOT}}^{DL}(\sigma \times \mathbf{m}) \\ &= H_K\left(\frac{H_{\text{SOT}}^{DL}}{H_K}\sin\beta m_y, -\frac{H_{\text{SOT}}^{DL}}{H_K}\sin\beta m_x + \frac{H_{\text{SOT}}^{DL}}{H_K}\cos\beta m_z,\right. \\ &\quad \left. -\frac{H_{\text{SOT}}^{DL}}{H_K}\cos\beta m_y + m_z\right). \end{aligned} \tag{5}$$

The direction of $\mathbf{H}_{\text{eff}}$ is also the finally stabilized direction of the magnetization as $J_{\text{SOT}} < J_c$. From Eqs. (4) and (5), we can then get

$$\begin{aligned} \frac{H_{\text{SOT}}^{DL}}{H_K}\sin\beta m_y &= k m_x, \\ -\frac{H_{\text{SOT}}^{DL}}{H_K}\sin\beta m_x + \frac{H_{\text{SOT}}^{DL}}{H_K}\cos\beta m_z &= k m_y, \\ -\frac{H_{\text{SOT}}^{DL}}{H_K}\cos\beta m_y + m_z &= k m_z, \end{aligned} \tag{6}$$

where the nonzero real number k satisfies

$$k^3 - k^2 + \left(\frac{H_{\text{SOT}}^{DL}}{H_K}\right)^2 k - \left(\frac{H_{\text{SOT}}^{DL}}{H_K}\right)^2 \sin^2\beta = 0. \tag{7}$$

From Eq. (7), we get $k = k(\frac{H_{\text{SOT}}^{DL}}{H_K}, \beta)$. Then the polar and azimuth angles (θ_H, φ_H) of the magnetization in the steady state can be obtained; the schematic diagram of polar angle θ_H and azimuth angle φ_H in spherical coordinates is shown in the upper left panel of Fig. 1.

$$\begin{aligned} \theta_H &= \arctan\left(\frac{(1-k)\sqrt{\sin^2\beta + \left(\frac{kH_K}{H_{\text{SOT}}^{DL}}\right)^2}}{k\cos\beta}\right), \\ \varphi_H &= \arctan\left(\frac{kH_K}{H_{\text{SOT}}^{DL}\sin\beta}\right). \end{aligned} \tag{8}$$

After getting θ_H and φ_H, we can transform the coordinate system from the original system O to a new one O' in which $\mathbf{H}_{\text{eff}}$ is directed at the z' axis, and the corresponding transformation matrix between the two coordinates is

$$R = \begin{pmatrix} \cos\theta_H & 0 & -\sin\theta_H \\ 0 & 1 & 0 \\ \sin\theta_H & 0 & \cos\theta_H \end{pmatrix}\begin{pmatrix} \cos\varphi_H & \sin\varphi_H & 0 \\ -\sin\varphi_H & \cos\varphi_H & 0 \\ 0 & 0 & 1 \end{pmatrix}. \tag{9}$$

And the relationship from the (x, y, z) coordinate to the (x', y', z') coordinate is simply

$$\begin{pmatrix} x' \\ y' \\ z' \end{pmatrix} = R\begin{pmatrix} x \\ y \\ z \end{pmatrix}. \tag{10}$$

The transformed coordination allows us to analyze the dynamic stability of systems straightforwardly. When $J_{\text{SOT}} < J_c$, the components of the magnetization along the x' and y' directions will converge to 0 after a long-enough damping, and as $J_{\text{SOT}} \geqslant J_c$, the precession amplitude will go divergently and the magnetization will switch to the opposite. At this time, the magnetization along the x' and y' components will gradually increase, which is our criterion to determine J_c. Similar methods to analyze the stability of dynamic systems [29–31,38] and even determine the critical current density for some other SOT modes [29–31] have also been adopted. Specifically, considering the two magnetization components along the x' and y' directions, we rewrite the LLG formula, Eq. (3), in the following Eq. (11):

$$-\frac{1+\alpha^2}{\gamma\mu_0}\frac{d}{dt}\begin{pmatrix} m_{x'} \\ m_{y'} \end{pmatrix} = \mathbf{M}\begin{pmatrix} m_{x'} \\ m_{y'} \end{pmatrix} + \mathbf{G}, \tag{11}$$

where $\mathbf{M}$ and $\mathbf{G}$ are 2×2 matrices, and their respective components are explicitly shown below:

$$\begin{aligned} M_{11} &= H_{\text{SOT}}^{DL}(-\sin\beta\cos^2\theta_H - \cos\theta_H\cos\varphi_H\cos\beta\sin\theta_H) + \alpha(\cos^4\theta_H - \cos^2\theta_H\sin^2\theta_H)H_K, \\ M_{12} &= -\alpha H_{\text{SOT}}^{DL}(\sin\beta\cos\theta_H + \cos\varphi_H\cos\beta\sin\theta_H) + \cos^3\theta_H H_K, \\ M_{21} &= \alpha H_{\text{SOT}}^{DL}(\sin\beta\cos\theta_H + \cos\varphi_H\cos\beta\sin\theta_H) + (\cos\theta_H\sin^2\theta_H - \cos^3\theta_H)H_K, \\ M_{22} &= H_{\text{SOT}}^{DL}(-\sin\beta\cos^2\theta_H - \cos\theta_H\cos\varphi_H\cos\beta\sin\theta_H) + \alpha\cos^4\theta_H H_K, \end{aligned} \tag{12}$$

$$\begin{aligned} G_1 &= -\alpha H_{SOT}^{DL}\cos\theta_H\cos\beta\sin\varphi_H - H_{\text{SOT}}^{DL}(\cos^3\theta_H\cos\varphi_H\cos\beta - \sin\beta\cos^2\theta_H\sin\theta_H) + \alpha\cos^4\theta_H\sin\theta_H H_k, \\ G_2 &= -\alpha H_{\text{SOT}}^{DL}(\cos^2\theta_H\cos\varphi_H\cos\beta - \sin\beta\cos\theta_H\sin\theta_H) - H_{\text{SOT}}^{DL}\cos^2\theta_H\cos\beta\sin\varphi_H - \cos^3\theta_H\sin\theta_H H_K. \end{aligned} \tag{13}$$

From Eq. (12), we can see that the eigenvalue of the 2×2 matrix $\mathbf{M}$ is $\lambda_{1,2} = \frac{M_{11}+M_{22}\pm i\sqrt{-4M_{12}M_{21}-(M_{11}-M_{22})^2}}{2}$. Worth noting, it can be proven that when $\frac{H_{\text{SOT}}^{DL}}{H_K} \ll 1$, eigenvalues of matrix $\mathbf{M}$ are complex. When $M_{11}+M_{22} < 0$, $m_{x'}$ and $m_{y'}$ decay to 0 with time if any; in contrast, when $M_{11}+M_{22} > 0$, they will diverge once the emergence of even a tiny $|m_{x'}|$ or $|m_{y'}|$ activated by thermal fluctuations or other reasons. Therefore, the switching criteria turns

$$M_{11} + M_{22} = 0. \tag{14}$$

The threshold current value J_c can be obtained from this condition. Detailed derivation steps are shown in the Appendix. If $\frac{H_{\text{SOT}}^{DL}}{H_K} \ll 1$ (widely applicable for most cases), we can get that

$$J_c = \frac{e\mu_0 M_s H_K t}{\hbar\theta_{SH}}\frac{4\alpha}{\sqrt{\sin^2\beta + 16\alpha^2\cos^2\beta} + \sin\beta}. \tag{15}$$

Worth noting, according to recent experiment data [22], two typical values of $\frac{H_{\text{SOT}}^{DL}}{H_K}$ are 0.014 and 0.023 at J_c, so the simplification condition $\frac{H_{\text{SOT}}^{DL}}{H_K} \ll 1$ reasonably holds here. When the

TABLE I. Parameters for numerical calculation (unless otherwise noted).

Parameters	Quantity	Value
Damping constant	α	0.015 [41]
Anisotropic field	$\mu_0 H_K$	0.85 T [40]
Saturated magnetization	M_s	1.3×10^6 A/m [40]
Ratio of anomalous SOT	$\tan\beta$	0.1 or 0.75 [20]
The FM thickness	t	1 nm
Overall spin Hall angle	θ_{SH}	0.075 [20]

out-of-plane torque is 0 or $\beta = 0$, the resultant $J_c = \frac{e\mu_0 M_s H_K t}{\hbar\theta_{SH}}$ becomes simplified in accord with the previously proposed J_c for the z-type SOT magnetization reversal at a small applied magnetic field [27,31,39]. More interesting, if $\frac{\alpha}{\tan\beta} \ll 1$ (e.g., a small damping in the order of 10^{-2} and a substantial anomalous SOT ratio not lower than ~0.1 can qualify the condition), the above equation can be simplified as

$$J_c = \frac{2e\mu_0 M_s H_K \alpha t}{\hbar\theta_{SH}\sin\beta}. \tag{16}$$

This threshold current density then shares a similar fashion with the case of the spin-transfer torque switching mode for the perpendicular MTJ with polarization **P** of the pinned layer replaced by the anomalous spin Hall angle $\theta_{SH}\sin\beta$. This reduced version also shares a similar fashion with the Y-type SOT mode [48].

III. RESULTS AND DISCUSSIONS

We visualize the magnetization trajectory with different out-of-plane torque ratio $\eta \equiv \tan\beta$ and $J_{\rm SOT}$, as shown in Fig. 2. Time step is set as $dt = 1$ fs. The initial direction of **m** is along the (0,0,1) in the O coordinate system. Simulation parameters are displayed in Table I [20,40,41]. For the situation without any out-of-plane SOT or $\eta = 0$, when $J_{\rm SOT} = 1.8 \times 10^{13}$ A m^{-2}, which is unable to destabilize the magnetization in the FM free layer, **m** is finally stabilized at the direction of the equivalent effective field (0.000, −0.451, 0.893). As $J_{\rm SOT} = 1.9 \times 10^{13}$ A m^{-2}, the SOT is large enough to destabilize **m** to (−1, 0, 0) in the equatorial plane as shown in Figs. 2(a) and 2(b). These scenarios produce the case of z-type mode without an external bias field. As for $\eta \neq 0$, the final state of $J_{\rm SOT} > J_c$ becomes different. From Eq. (15), we can directly calculate that the threshold currents for $\eta = 0.1$ and 0.75 are $J_c = 6.23 \times 10^{12}$ A m^{-2} and 1.116×10^{12} A m^{-2}, respectively. As $J_{\rm SOT} = 6.2 \times 10^{12}$ A m^{-2} and 1.1×10^{12} A m^{-2} for $\eta = 0.1$ and 0.75, respectively, the SOT acting on the FM free layer is not large enough, so the precession amplitude gets smaller and smaller, and finally **m** is stabilized at the direction of $\mathbf{H}_{\rm eff}$ (0.001, −0.1430, 0.9897) and (0.0030, −0.0234, 0.9997) for $\eta = 0.1$ and 0.75, respectively [see Figs. 2(c) and 2(e)]. When $J_{\rm SOT} = 6.37 \times 10^{12}$ A m^{-2} and 1.12×10^{12} A m^{-2} for $\eta = 0.1$ and 0.75, respectively, the precession amplitude is divergently increasing, and **m** eventually turns to the opposite direction (−0.0021, 0.1432, −0.9897) and (0.0003, 0.0200, −0.9998) for $\eta = 0.1$ and 0.75, respectively, as shown in Figs. 2(d) and 2(f), consistent with our previous analysis. Worth mentioning, as $J_{\rm SOT} > J_c$, **m** will not converge to the direction of $\mathbf{H}_{\rm eff}$ since the prerequisite for the calculation is $|m'_x|, |m'_y| \ll 1$, which is violated in this case. This notice does not undermine the strictness of the criteria of deriving J_c. We show the η dependence of the analytical threshold $J_C^{\rm ana}$, the numerical simulation threshold $J_C^{\rm num}$, and the relative error $\delta J_C/J_C^{\rm num} = (J_C^{\rm num} - J_C^{\rm ana})/J_C^{\rm num}$ in Fig. 2(g). The analytical model predicts an accurate J_C within 3% error for $\eta \geqslant 0.1$ and even better resolution within 0.5% for $\eta \geqslant 0.2$. This figure proves the high consistency between the analytical and the simulation models.

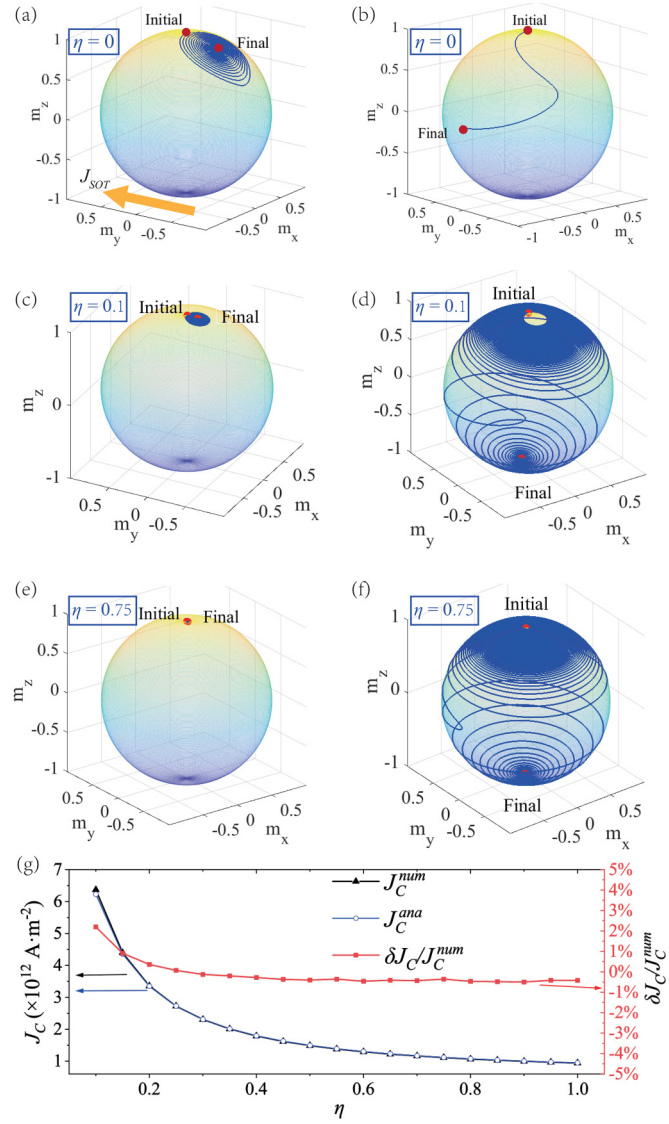

FIG. 2. (a)–(f) The magnetization trajectory with different η and $J_{\rm SOT}$. The two parameters are shown as follows. $\eta = 0$, (a) $J_{\rm SOT} = 1.8 \times 10^{13}$ A m^{-2} and (b) $J_{\rm SOT} = 1.9 \times 10^{13}$ A m^{-2}; $\eta = 0.1$, with threshold current value $J_c = 6.23 \times 10^{12}$ A m^{-2}, (c) $J_{\rm SOT} = 6.2 \times 10^{12}$ A m^{-2}, and (d) $J_{\rm SOT} = 6.37 \times 10^{12}$ A m^{-2}; $\eta = 0.75$, with threshold current value $J_c = 1.116 \times 10^{12}$ A m^{-2}, (e) $J_{\rm SOT} = 1.1 \times 10^{12}$ A m^{-2}, and (f) $J_{\rm SOT} = 1.12 \times 10^{12}$ A m^{-2}. (g) The η dependence of analytical threshold current $J_C^{\rm ana}$, numerical threshold current $J_C^{\rm num}$, and error $\delta J_C/J_C^{\rm num} = (J_C^{\rm num} - J_C^{\rm ana})/J_C^{\rm num}$.

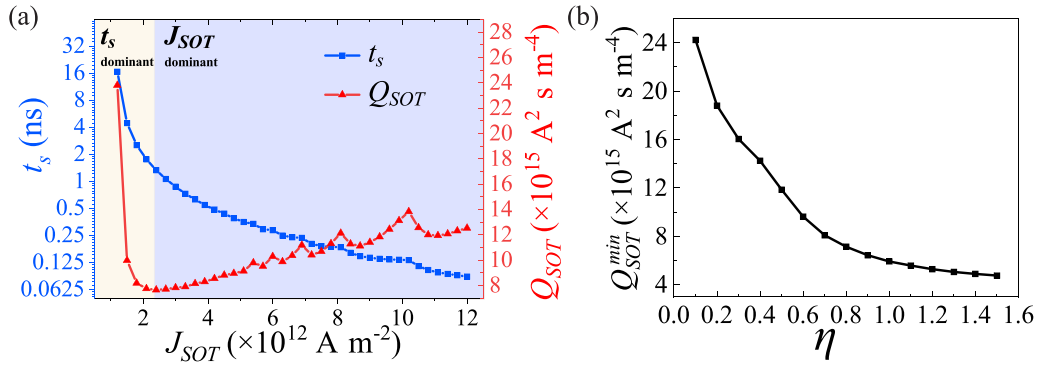

FIG. 3. (a) The J_{SOT} dependence of the switching time t_s and the switching energy consumption Q_{SOT}. (b) The η dependence of minimum energy loss $Q_{\mathrm{SOT}}^{\mathrm{min}}$. In the regime of $\eta \leqslant 0.8$, the increase in η can significantly reduce the value of $Q_{\mathrm{SOT}}^{\mathrm{min}}$.

We also calculate the relationship between the switching time t_s, switching energy consumption Q_{SOT}, and J_{SOT} when $J_{\mathrm{SOT}} > J_c$. Here $\eta = 0.75$ and t_s is defined as the time from sourcing current to the occurrence of a negative m_z component in the calculation. The switching energy consumption is defined as $Q_{\mathrm{SOT}} \equiv J_{\mathrm{SOT}}^2 t_s$, which scales with the energy consumed in the switching process. We can see from Fig. 3(a) that as J_{SOT} increases, $t_s$decreases rapidly from 16.5 ns at $J_{\mathrm{SOT}} = 1.2 \times 10^{12}$ A m^{-2} to 0.1 ns at $J_{\mathrm{SOT}} = 1.11 \times 10^{13}$ A m^{-2}, and the influence of J_{SOT} on t_s is then gradually reduced as J_{SOT} increases further. Figure 3(a) also shows that Q_{SOT} minimizes when J_{SOT} is near 2.4×10^{12} A m^{-2}, with the minimum value $Q_{\mathrm{SOT}}^{\mathrm{min}} = 7.7 \times 10^{15}$ A^2 s m^{-4}. Then we study the η dependence of $Q_{\mathrm{SOT}}^{\mathrm{min}}$, as shown in Fig. 3(b). As η increases, $Q_{\mathrm{SOT}}^{\mathrm{min}}$ gradually decreases, manifesting the larger out-of-plane torque ratio that results in less energy consumption. With a resistivity of the writing channel $\rho = 200$ μΩ cm [20] and the SOT-channel width $l = 100$ nm and length $d = 300$ nm, $Q_{\mathrm{SOT}} = 1 \times 10^{15}$ A^2 s m^{-4} corresponds to an energy consumption of 0.06 pJ. So the minimal energy consumption under the used parameters is about 0.46 pJ at $\eta = 0.75$, $J_{\mathrm{SOT}} = 2.7 \times 10^{12}$ A m^{-2}; correspondingly, the switching time is about 1 ns.

Then, we numerically calculate the dependence of J_c on the anisotropy strength H_K, out-of-plane torque ratio η, FM free-layer thickness t, and Gilbert damping constant α, as shown in Fig. 4. We can see that J_c increases with the increase in H_K as expected. In addition, we can also see from Fig. 4(a) that J_c gradually decreases with the increase in η. This is because the decisive factor that affects magnetization switching is the z component of anomalous SOT. When the z component of the effective field caused by SOT is larger than effective anisotropy field, magnetization switch happens. And as η increases, the z component of SOT increases, then J_c becomes lower if we still intend to switch the magnetization. We extract three threshold currents corresponding to different anisotropic properties, as shown in Fig. 4(b). Clearly shown in the figure, the higher anisotropy results in the greater influence of η on J_c.

We also study the thickness t and Gilbert damping α dependencies of J_c, as shown in Fig. 4(c). As α increases, J_c increases. This feature, similar to the classic spin-transfer torque (STT) switching scheme [42–45], can be explained as follows. In the switching process, the competition between the intrinsic damping term and the anti-damping-like SOT term dominates the switching result. If the intrinsic damping term overwhelms the SOT term, the magnetization will finally stabilize at somewhere close to the initial position (the position as $J_{\mathrm{SOT}} = 0$) as in Figs. 2(a), 2(c), and 2(e). Only when SOT provides a larger anti-damping-like torque than the intrinsic damping, can the switching occur as shown in Figs. 2(b), 2(d), and 2(f). This switching mode is therefore so-called damping-dominated spin dynamics in contrast to those precession-dominated ones such as the voltage-controllable magnetic anisotropy-induced switching [46,47]. As a typical and characteristic feature of the damping-dominated switching, the current threshold J_c should be proportional to the damping constant α of a system since a larger α makes a system consume more energy via the Gilbert damping in the switching process and further the more dissipated energy has to be compensated by a larger current. And as the thickness of the magnetic layer is higher, J_c becomes larger too with no doubt in accordance with Eq. (15). Because the total number of magnetic moments in the magnetic layer is proportional

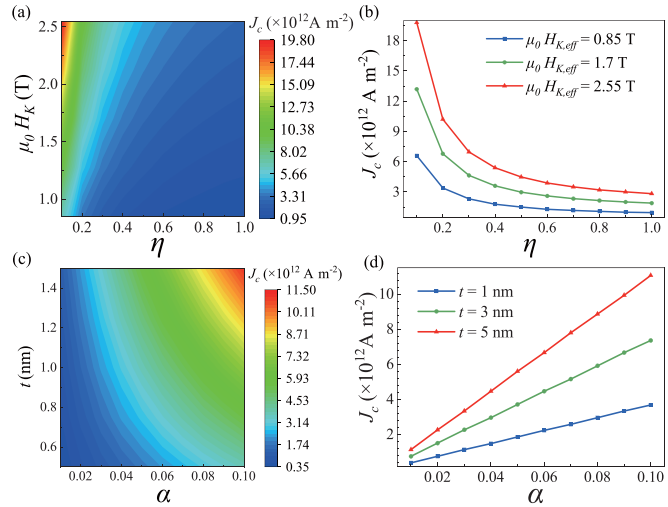

FIG. 4. (a) The dependence of J_c on the anisotropic field H_K and anomalous ratio η. (b) The η dependence of J_c under $\alpha = 0.015$, $t = 1$ nm extracted from Fig. 4(a). (c) The dependence of J_c on the thickness t and Gilbert damping α. (d) The η dependence of J_c under $\mu_0 H_K = 0.85$ T, $\eta = 0.75$ extracted from Fig. 4(c).

to the thickness t of the magnetic layer, the average SOT imposed to each moment is thus inversely proportional to t in accordance with Eq. (2) $H_{\rm SOT}^{DL} = \frac{J_{\rm SOT}\theta_{SH}\hbar}{2et\mu_0 M_s}$ and also Eq. (3) in Ref. [36]. When t increases, J_c should also increase to ensure the average SOT imposed on each moment to reach the threshold. Therefore, J_c is proportional to the thickness of the magnetic layer as expected. We then extract three J_c corresponding to different thicknesses, as shown in Fig. 4(d). J_c scales linearly with α, also in accordance with Eq. (15) and the STT scheme. Worth noting, on the other hand, when $\eta = 0$, the threshold current, Eq. (15), is equal to the threshold current for the z-type SOT mode with an applied magnetic field $H_x = 0$. The threshold current for the z-type SOT magnetization switching is [31]

$$J_c = \frac{et\mu_0 M_s H_K}{\hbar\theta_{SH}}\left[\frac{\sqrt{4\alpha\left[4\alpha+2\alpha\left(\frac{H_{\rm SOT}^{FL}}{H_{\rm SOT}^{DL}}\right)^2+\frac{H_{\rm SOT}^{FL}}{H_{\rm SOT}^{DL}}\right]+\left[9\alpha^2-4\alpha\left(\frac{H_{\rm SOT}^{FL}}{H_{\rm SOT}^{DL}}\right)-8\left(\alpha\frac{H_{\rm SOT}^{FL}}{H_{\rm SOT}^{DL}}\right)^2\right]\left(\frac{H_x}{H_K}\right)^2}}{4\alpha+2\alpha\left(\frac{H_{\rm SOT}^{FL}}{H_{\rm SOT}^{DL}}\right)^2+\left(\frac{H_{\rm SOT}^{FL}}{H_{\rm SOT}^{DL}}\right)}-\frac{5\alpha\frac{H_x}{H_K}}{4\alpha+2\alpha\left(\frac{H_{\rm SOT}^{FL}}{H_{\rm SOT}^{DL}}\right)^2+\left(\frac{H_{\rm SOT}^{FL}}{H_{\rm SOT}^{DL}}\right)}\right] \quad (17)$$

with fieldlike torque intensity $H_{\rm SOT}^{FL}$ and applied magnetic field H_x. When $H_{\rm SOT}^{FL} = 0$ and $H_x \ll H_K$, the threshold current is [27]

$$J_c = \frac{et\mu_0 M_s}{\hbar\theta_{SH}}(H_K - \sqrt{2}H_x). \quad (18)$$

The experiment [25] and the above derivation have shown that the anomalous SOT can switch the magnetization of FM free layer if the applied current is above the threshold J_c. However, even if $J_{\rm SOT} < J_c$, the anomalous SOT can still manifest itself by acting an effective exchange bias field $H_{\rm bias}$, which facilitates us to determine the anomalous SOT efficiency. We calculate the hysteresis loops corresponding to different $J_{\rm SOT} < J_c$, as shown in Fig. 5(a). Here the LLGS equation has to take magnetic field $\mathbf{H}_z$ into account.

$$\frac{\partial \mathbf{m}}{\partial t} = -\gamma\mu_0[\mathbf{m}\times(\mathbf{H_K}+\mathbf{H_z})]+\alpha\left(\mathbf{m}\times\frac{\partial \mathbf{m}}{\partial t}\right) + \gamma\mu_0 H_{\rm SOT}^{DL}[(\mathbf{m}\times\sigma)\times\mathbf{m}]. \quad (19)$$

Figure 5(a) shows for an unbiased loop without $J_{\rm SOT}$, the forward and backward switching coercivity of the FM layer is symmetric. However, when a positive (negative) $J_{SOT,0} = 6.28\times10^{11}$ A m^{-2} is applied, the hysteresis loop is biased leftward (rightward) or their H_z-symmetrical axis is offset toward the negative (positive) direction. Therefore, equivalently, a nonzero $J_{\rm SOT}$ imposes an exchange bias field $H_{\rm bias}$ along the z axis to the FM free layer, which determines the switching direction in the field-free condition. Compared to the z-type SOT [39] mode that biases hysteresis loops with the help of an in-plane magnetic field, this result gives an alternative biasing method to control magnetization of the FM layer, which is easier to implement. We also calculate the dependence of $H_{\rm bias}$ on $J_{\rm SOT}$ shown in Fig. 5(b), which turns out linear with each other and the slope is $\frac{\hbar\theta_{SH}\sin\beta}{2e\mu_0\alpha t M_s} = 6.05\times10^{-7}$ m, if $\frac{H_{\rm SOT}^{DL}}{H_K} \ll 1$ and $\frac{H_{\rm bias}}{H_K} \ll 1$. This result provides a direct way to determine the anomalous torque efficiency. Compared with the threshold trend that evidences the anomalous torque in magnetic trilayers [13], our results show a straightforward linear relationship between $H_{\rm bias}$ and $J_{\rm SOT}$. This discrepancy can probably be induced by complex domain structures in those micrometer-sized Hall bar devices; however, essentially, the abnormal torque only induces a linear-to-current effective field in the coherent switching mode. Thus we expect this linear dependence can be directly observed, for instance, in a sub-100-nm-sized magnetic tunnel junction.

Our model gives an analytic J_c [see Eq. (15)] for the anomalous SOT mode with both in-plane and out-of-plane spin current polarization components for switching a perpendicular magnet. In the case of $\eta \gg 1$ ($\beta = 90^\circ$), our work naturally converges to the J_C of the y-type mode as reported in [48], which demonstrates the validity of the model. In addition, the derived J_C can also be used to predict the $X-Y$ mixed SOT mode [48] and the STT+SOT combined switching mode [28,49], in which a spin current with polarization along the easy axis and another spin current with polarization perpendicular to the easy axis both exist. Therefore, our analytic result is also instructive for SOT devices designed based on the $X-Y$ mixed mode and the STT+SOT mode.

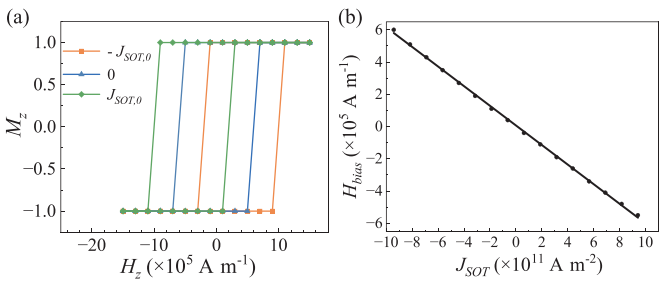

FIG. 5. (a) Hysteresis loop of FM free layer under different applied currents $J_{\rm SOT}$. (b) Relationship between equivalent exchange bias field $H_{\rm bias}$ and applied current $J_{\rm SOT}$. Here $\eta = 0.75$.

IV. CONCLUSIONS

In this paper, we present an analytical derivation of the threshold current required to achieve field-free switching of perpendicular magnetization using the anomalous SOT in combination with an ordinary one. We also conduct numerical simulations to investigate the magnetization trajectory of a FM free layer when the applied current is both below and above the threshold. Our analytical and numerical results in J_C are in agreement with less than 3% errors. Furthermore, we explore the dependence of the switching time and energy consumption on the applied current and show that the minimum energy consumption is negatively correlated with the

out-of-plane torque proportion. Additionally, we investigate the effects of various parameters, including anisotropy strength, out-of-plane torque ratio, FM free-layer thickness, and Gilbert damping constant, on the threshold current. Our findings indicate a negative correlation between the out-of-plane torque proportion and the threshold current, and a positive correlation between the other three parameters and the threshold current. Finally, we demonstrate that when the applied current is below the threshold, it can induce an exchange bias field H_{bias} imposed on the FM free layer. Our numerical results show that the exchange bias field H_{bias} is proportional to the applied current J_{SOT} for the coherent switching dynamics. This study provides insights into the design of spintronic devices that enable field-free switching of perpendicular magnetization using the anomalous spin-orbit torque, and offers a direct method for adjusting the exchange bias field, which can be useful in controlling FM layer magnetization pinning and depinning.

ACKNOWLEDGMENTS

This work is financially supported by the National Key Research and Development Program of China (MOST) (Grants No. 2022YFA1402800 and No. 2017YFA0206200), the National Natural Science Foundation of China (NSFC) (Grants No. 12134017,11974398 and No. 12061131012), and partially supported by the Strategic Priority Research Program (B) [Grant No. XDB33000000, Youth Innovation Promotion Association of CAS (2020008)].

APPENDIX: DERIVATION OF EQ. (15)

From Eq. (7), suppose $k_1 = k - \frac{1}{3}$; we can get

$$k_1^3+\left[\left(\frac{H_{\text{SOT}}^{DL}}{H_K}\right)^2-\frac{1}{3}\right]k_1+\left[-\frac{2}{27}+\left(\frac{1}{3}-\sin^2\beta\right)\left(\frac{H_{\text{SOT}}^{DL}}{H_K}\right)^2\right]=0. \tag{A1}$$

If $\frac{H_{\text{SOT}}^{DL}}{H_K} \ll 1$, we can get

$$\begin{aligned} k_1 &= \sqrt[3]{\frac{1}{27}-\frac{1-3\sin^2\beta}{6}\left(\frac{H_{\text{SOT}}^{DL}}{H_K}\right)^2+\frac{\sin\beta}{3\sqrt{3}}\frac{H_{\text{SOT}}^{DL}}{H_K}} \\ &\quad+\sqrt[3]{\frac{1}{27}-\frac{1-3\sin^2\beta}{6}\left(\frac{H_{\text{SOT}}^{DL}}{H_K}\right)^2-\frac{\sin\beta}{3\sqrt{3}}\frac{H_{\text{SOT}}^{DL}}{H_K}} \\ &= \frac{2}{3}-\cos^2\beta\left(\frac{H_{\text{SOT}}^{DL}}{H_K}\right)^2, \end{aligned} \tag{A2}$$

so that

$$k = 1-\cos^2\beta\left(\frac{H_{\text{SOT}}^{DL}}{H_K}\right)^2. \tag{A3}$$

We can get the pole angle and azimuth angle (θ_H, φ_H):

$$\begin{aligned} \tan\theta_H &= \frac{(1-k)\sqrt{\sin^2\beta+\left(kH_K/H_{\text{SOT}}^{DL}\right)^2}}{k\cos\beta} \\ &= \cos\beta\frac{H_{\text{SOT}}^{DL}}{H_K} \\ \cos\varphi_H &= \frac{\sin\beta H_{\text{SOT}}^{DL}/H_K}{\sqrt{1-\left(\cos\beta H_K/H_{\text{SOT}}^{DL}\right)^2+\left(\sin\beta H_K/H_{\text{SOT}}^{DL}\right)^2}} \\ &= \sin\beta\frac{H_{\text{SOT}}^{DL}}{H_K}. \end{aligned} \tag{A4}$$

From Eq. (12), we can get threshold current using equation $M_{11}+M_{22}=0$:

$$J_c=\frac{et\mu_0 M_s H_K}{\theta_{SH}\hbar}\frac{4\alpha}{\sqrt{\sin^2\beta+16\alpha^2\cos^2\beta}+\sin\beta}. \tag{A5}$$

[1] W. J. Kong, C. H. Wan, C. Y. Guo, C. Fang, B. S. Tao, X. Wang, and X. F. Han, All-electrical manipulation of magnetization in magnetic tunnel junction via spin–orbit torque, Appl. Phys. Lett. **116**, 162401 (2020).

[2] A. Manchon, J. Železný, I. M. Miron, T. Jungwirth, J. Sinova, A. Thiaville, K. Garello, and P. Gambardella, Current-induced spin-orbit torques in ferromagnetic and antiferromagnetic systems, Rev. Mod. Phys. **91**, 035004 (2019).

[3] I. Mihai Miron, G. Gaudin, S. Auffret, B. Rodmacq, A. Schuhl, S. Pizzini, J. Vogel, and P. Gambardella, Current-driven spin torque induced by the Rashba effect in a ferromagnetic metal layer, Nat. Mater. **9**, 230 (2010).

[4] J. Sinova, S. O. Valenzuela, J. Wunderlich, C. H. Back, and T. Jungwirth, Spin Hall effects, Rev. Mod. Phys. **87**, 1213 (2015).

[5] C. Song, R. Zhang, L. Liao, Y. Zhou, X. Zhou, R. Chen, Y. You, X. Chen, and F. Pan, Spin-orbit torques: Materials, mechanisms, performances, and potential applications, Prog. Mater. Sci. **118**, 100761 (2021).

[6] Q. Zhang, K. S. Chan, and J. Li, Spin-transfer torque generated in graphene based topological insulator heterostructures, Sci. Rep. **8**, 4343 (2018).

[7] A. Brataas, A. D. Kent, and H. Ohno, Current-induced torques in magnetic materials, Nat. Mater. **11**, 372 (2012).

[8] L. Liu, O. J. Lee, T. J. Gudmundsen, D. C. Ralph, and R. A. Buhrman, Current-Induced Switching of Perpendicularly Magnetized Magnetic Layers Using Spin Torque from the Spin Hall Effect, Phys. Rev. Lett. **109**, 096602 (2012).

[9] L. Liu, C.-F. Pai, Y. Li, H. W. Tseng, D. C. Ralph, and R. A. Buhrman, Spin-torque switching with the giant spin Hall effect of tantalum, Science **336**, 555 (2012).

[10] S. Chen, J. Yu, Q. Xie, X. Zhang, W. Lin, L. Liu, J. Zhou, X. Shu, R. Guo, Z. Zhang, and J. Chen, Free field electric switching of perpendicularly magnetized thin film by spin current gradient, ACS Appl. Mater. Interfaces **11**, 30446 (2019).

[11] G. Yu, P. Upadhyaya, Y. Fan, J. G. Alzate, W. Jiang, K. L. Wong, S. Takei, S. A. Bender, L.-T. Chang, Y. Jiang, M. Lang, J. Tang, Y. Wang, Y. Tserkovnyak, P. K. Amiri, and K. L. Wang,

Switching of perpendicular magnetization by spin–orbit torques in the absence of external magnetic fields, Nat. Nanotechnol. **9**, 548 (2014).

[12] Y. Liu, Y. Liu, M. Chen, S. Srivastava, P. He, K. L. Teo, T. Phung, S.-H. Yang, and H. Yang, Current-Induced Out-of-plane Spin Accumulation on the (001) Surface of the $IrMn_3$ Antiferromagnet, Phys. Rev. Appl. **12**, 064046 (2019).

[13] S.-h. C. Baek, V. P. Amin, Y.-W. Oh, G. Go, S.-J. Lee, G.-H. Lee, K.-J. Kim, M. D. Stiles, B.-G. Park, and K.-J. Lee, Spin currents and spin–orbit torques in ferromagnetic trilayers, Nat. Mater. **17**, 509 (2018).

[14] S. Fukami, C. Zhang, S. DuttaGupta, A. Kurenkov, and H. Ohno, Magnetization switching by spin–orbit torque in an antiferromagnet–ferromagnet bilayer system, Nat. Mater. **15**, 535 (2016).

[15] W. J. Kong, C. H. Wan, X. Wang, B. S. Tao, L. Huang, C. Fang, C. Y. Guo, Y. Guang, M. Irfan, and X. F. Han, Spin–orbit torque switching in a T-type magnetic configuration with current orthogonal to easy axes, Nat. Commun. **10**, 233 (2019).

[16] Y.-C. Lau, D. Betto, K. Rode, J. M. D. Coey, and P. Stamenov, Spin–orbit torque switching without an external field using interlayer exchange coupling, Nat. Nanotechnol. **11**, 758 (2016).

[17] Y.-W. Oh, S.-h. Chris Baek, Y. M. Kim, H. Y. Lee, K.-D. Lee, C.-G. Yang, E.-S. Park, K.-S. Lee, K.-W. Kim, G. Go, J.-R. Jeong, B.-C. Min, H.-W. Lee, K.-J. Lee, and B.-G. Park, Field-free switching of perpendicular magnetization through spin–orbit torque in antiferromagnet/ferromagnet/oxide structures, Nat. Nanotechnol. **11**, 878 (2016).

[18] W. He, C. Wan, C. Zheng, Y. Wang, X. Wang, T. Ma, Y. Wang, C. Guo, X. Luo, M. E. Stebliy, G. Yu, Y. Liu, A. V. Ognev, A. S. Samardak, and X. Han, Field-free spin-orbit torque switching enabled by the interlayer Dzyaloshinskii-Moriya interaction, Nano Lett. **22**, 6857 (2022).

[19] D. MacNeill, G. M. Stiehl, M. H. D. Guimarães, N. D. Reynolds, R. A. Buhrman, and D. C. Ralph, Thickness dependence of spin-orbit torques generated by WTe_2, Phys. Rev. B **96**, 054450 (2017).

[20] H. Bai, X. F. Zhou, H. W. Zhang, W. W. Kong, L. Y. Liao, X. Y. Feng, X. Z. Chen, Y. F. You, Y. J. Zhou, L. Han, W. X. Zhu, F. Pan, X. L. Fan, and C. Song, Control of spin-orbit torques through magnetic symmetry in differently oriented noncollinear antiferromagnetic Mn_3Pt, Phys. Rev. B **104**, 104401 (2021).

[21] D. Go, M. Sallermann, F. R. Lux, S. Blugel, O. Gomonay, and Y. Mokrousov, Noncollinear Spin Current for Switching of Chiral Magnetic Textures, Phys. Rev. Lett. **129**, 097204 (2022).

[22] I. H. Kao, R. Muzzio, H. Zhang, M. Zhu, J. Gobbo, S. Yuan, D. Weber, R. Rao, J. Li, J. H. Edgar, J. E. Goldberger, J. Yan, D. G. Mandrus, J. Hwang, R. Cheng, J. Katoch, and S. Singh, Deterministic switching of a perpendicularly polarized magnet using unconventional spin-orbit torques in WTe_2, Nat. Mater. **21**, 1029 (2022).

[23] Y. Liu, B. Zhou, Z. Dai, E. Zhang, and J.-g. Zhu, Iridium enabled field-free spin-orbit torque switching of perpendicular magnetic tunnel junction device, arXiv:1911.05007.

[24] J. Zhou, X. Shu, Y. Liu, X. Wang, W. Lin, S. Chen, L. Liu, Q. Xie, T. Hong, P. Yang, B. Yan, X. Han, and J. Chen, Magnetic asymmetry induced anomalous spin-orbit torque in IrMn, Phys. Rev. B **101**, 184403 (2020).

[25] L. Liu, C. Zhou, X. Shu, C. Li, T. Zhao, W. Lin, J. Deng, Q. Xie, S. Chen, J. Zhou, R. Guo, H. Wang, J. Yu, S. Shi, P. Yang, S. Pennycook, A. Manchon, and J. Chen, Symmetry-dependent field-free switching of perpendicular magnetization, Nat. Nanotechnol. **16**, 277 (2021).

[26] M. DC, D.-F. Shao, V. D. H. Hou, A. Vailionis, P. Quarterman, A. Habiboglu, M. B. Venuti, F. Xue, Y.-L. Huang, C.-M. Lee, M. Miura, B. Kirby, C. Bi, X. Li, Y. Deng, S.-J. Lin, W. Tsai, S. Eley, W.-G. Wang, J. A. Borchers, E. Y. Tsymbal, and S. X. Wang, Observation of anti-damping spin–orbit torques generated by in-plane and out-of-plane spin polarizations in $MnPd_3$, Nat. Mater. **22**, 591 (2023).

[27] K.-S. Lee, S.-W. Lee, B.-C. Min, and K.-J. Lee, Threshold current for switching of a perpendicular magnetic layer induced by spin Hall effect, Appl. Phys. Lett. **102**, 112410 (2013).

[28] J. Z. Sun, Spin-current interaction with a monodomain magnetic body: A model study, Phys. Rev. B **62**, 570 (2000).

[29] T. Taniguchi, S. Mitani, and M. Hayashi, Critical current destabilizing perpendicular magnetization by the spin Hall effect, Phys. Rev. B **92**, 024428 (2015).

[30] T. Taniguchi and H. Kubota, Instability analysis of spin-torque oscillator with an in-plane magnetized free layer and a perpendicularly magnetized pinned layer, Phys. Rev. B **93**, 174401 (2016).

[31] D. Zhu and W. Zhao, Threshold Current Density for Perpendicular Magnetization Switching Through Spin-Orbit Torque, Phys. Rev. Appl. **13**, 044078 (2020).

[32] T. L. Gilbert, Classics in magnetics a phenomenological theory of damping in ferromagnetic materials, IEEE Trans. Magn. **40**, 3443 (2004).

[33] K. Garello, I. M. Miron, C. O. Avci, F. Freimuth, Y. Mokrousov, S. Blügel, S. Auffret, O. Boulle, G. Gaudin, and P. Gambardella, Symmetry and magnitude of spin–orbit torques in ferromagnetic heterostructures, Nat. Nanotechnol. **8**, 587 (2013).

[34] A. V. Khvalkovskiy, V. Cros, D. Apalkov, V. Nikitin, M. Krounbi, K. A. Zvezdin, A. Anane, J. Grollier, and A. Fert, Matching domain-wall configuration and spin-orbit torques for efficient domain-wall motion, Phys. Rev. B **87**, 020402(R) (2013).

[35] J. Kim, J. Sinha, M. Hayashi, M. Yamanouchi, S. Fukami, T. Suzuki, S. Mitani, and H. Ohno, Layer thickness dependence of the current-induced effective field vector in Ta|CoFeB|MgO, Nat. Mater. **12**, 240 (2013).

[36] C.-F. Pai, M.-H. Nguyen, C. Belvin, L. H. Vilela-Leão, D. C. Ralph, and R. A. Buhrman, Enhancement of perpendicular magnetic anisotropy and transmission of spin-Hall-effect-induced spin currents by a Hf spacer layer in W/Hf/CoFeB/MgO layer structures, Appl. Phys. Lett. **104**, 082407 (2014).

[37] J. Park, G. E. Rowlands, O. J. Lee, D. C. Ralph, and R. A. Buhrman, Macrospin modeling of sub-ns pulse switching of perpendicularly magnetized free layer via spin-orbit torques for cryogenic memory applications, Appl. Phys. Lett. **105**, 102404 (2014).

[38] H. Sayama, *Linear Stability Analysis of Nonlinear Dynamical Systems* (Binghamton University, State University of New York, New York, 2023), Vol. 7.5.1.

[39] X. Han, X. Wang, C. Wan, G. Yu, and X. Lv, Spin-orbit torques: Materials, physics, and devices, Appl. Phys. Lett. **118**, 120502 (2021).

[40] G. W. Kim, A. S. Samardak, Y. J. Kim, I. H. Cha, A. V. Ognev, A. V. Sadovnikov, S. A. Nikitov, and Y. K. Kim, Role of the

Heavy Metal's Crystal Phase in Oscillations of Perpendicular Magnetic Anisotropy and the Interfacial Dzyaloshinskii-Moriya Interaction in W/Co-Fe-B/MgO Films, Phys. Rev. Appl. **9**, 064005 (2018).

[41] J. Lourembam, A. Ghosh, M. Zeng, S. K. Wong, Q. J. Yap, and S. T. Lim, Thickness-Dependent Perpendicular Magnetic Anisotropy and Gilbert Damping in Hf/$Co_{20}Fe_{60}B_{20}$/MgO Heterostructures, Phys. Rev. Appl. **10**, 044057 (2018).

[42] S. Bhatti, R. Sbiaa, A. Hirohata, H. Ohno, S. Fukami, and S. N. Piramanayagam, Spintronics based random access memory: A review, Mater. Today **20**, 530 (2017).

[43] T. Chirac, J.-Y. Chauleau, P. Thibaudeau, O. Gomonay, and M. Viret, Ultrafast antiferromagnetic switching in NiO induced by spin transfer torques, Phys. Rev. B **102**, 134415 (2020).

[44] C. Jia, D. Ma, A. F. Schäffer, and J. Berakdar, Twisted magnon beams carrying orbital angular momentum, Nat. Commun. **10**, 2077 (2019).

[45] I. M. Miron, K. Garello, G. Gaudin, P.-J. Zermatten, M. V. Costache, S. Auffret, S. Bandiera, B. Rodmacq, A. Schuhl, and P. Gambardella, Perpendicular switching of a single ferromagnetic layer induced by in-plane current injection, Nature (London) **476**, 189 (2011).

[46] Y. Shiota, T. Nozaki, F. Bonell, S. Murakami, T. Shinjo, and Y. Suzuki, Induction of coherent magnetization switching in a few atomic layers of FeCo using voltage pulses, Nat. Mater. **11**, 39 (2012).

[47] R. Matsumoto, T. Nozaki, S. Yuasa, and H. Imamura, Voltage-Induced Precessional Switching at Zero-Bias Magnetic Field in a Conically Magnetized Free Layer, Phys. Rev. Appl. **9**, 014026 (2018).

[48] S. Fukami, T. Anekawa, C. Zhang, and H. Ohno, A spin–orbit torque switching scheme with collinear magnetic easy axis and current configuration, Nat. Nanotechnol. **11**, 621 (2016).

[49] J. Z. Sun, Spin-transfer torque switching probability of CoFeB/MgO/CoFeB magnetic tunnel junctions beyond macrospin, Phys. Rev. B **104**, 104428 (2021).